Science of the Total Environment 807 (2022) 150756

Contents lists available at ScienceDirect

Science of the Total Environment

journal homepage: www.elsevier.com/locate/scitotenv

Insights into recent aerosol trends over Asia from observations and CMIP6 simulations

S. Ramachandran [a,b,*], Maheswar Rupakheti [b], R. Cherian [c]

[a] Physical Research Laboratory, Ahmedabad, India
[b] Institute for Advanced Sustainability Studies, Potsdam, Germany
[c] Leipzig Institute for Meteorology, University of Leipzig, Leipzig, Germany

HIGHLIGHTS

- Aerosol trends over Asia analyzed from observations and CMIP6 model simulations.
- Models are not able to capture the observed magnitudes and trends in aerosols.
- Observations exhibit a dipole in aerosol optical depth over Asia.
- Model simulations show that aerosol-induced atmospheric heating increases over Asia.
- Results have implications to regional, global and decadal climate change.

GRAPHICAL ABSTRACT

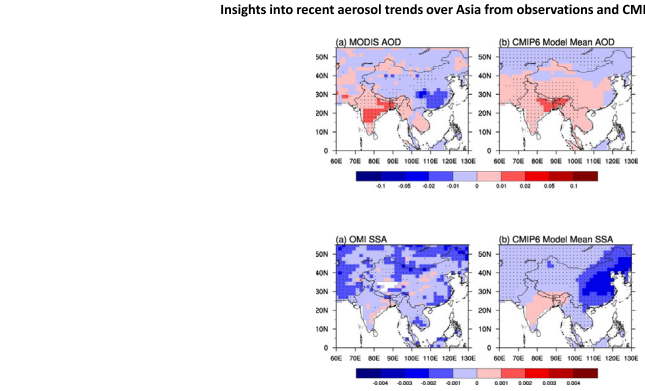

ARTICLE INFO

Article history:
Received 22 July 2021
Received in revised form 3 September 2021
Accepted 29 September 2021
Available online 4 October 2021

Editor: Pavlos Kassomenos

Keywords:
Atmospheric aerosols
Asia
Trends
Observations
CMIP6 simulations
Implications

ABSTRACT

Aerosols continue to contribute the largest uncertainty in climate change. Over Asia, a global aerosol hotspot, spatial patterns of aerosol emissions are changing mainly because of changes in anthropogenic emissions, producing a dipole in atmospheric aerosol loading between East (decrease in emissions) and South Asia (increase in emissions). The resultant aerosol radiative effects are expected to be different as compared to the last decades of the 20th century because of this emerging Asian aerosol dipole. The projection and assessments of radiative and climate impacts of aerosols rely on simulating accurately the aerosol properties, thus, making it imperative that current climate models involved in climate assessments including the Intergovernmental Panel on Climate Change Assessment Reports, simulate well the magnitude and trends in changing aerosol properties. For the first time, in this study we analyze trends in aerosol properties over Asia from satellite and ground-based observations, and simulations from climate models in Coupled Model Intercomparison Project Phase 6 (CMIP6) experiment with state-of-the-art treatment of aerosol chemistry, physics and meteorology. The results reveal large inter-model differences in model estimates, and discrepancies between model simulations and observations as most models are not able to capture the recent observed magnitudes and trends in aerosol optical depth (AOD) and single scattering albedo (SSA) over Asia. The absolute and the relative (percent) trends (positive and/or negative) in AOD are significantly higher than the trends in SSA. The aerosol-induced effective radiative forcing within the atmosphere simulated with three CMIP6 models show a positive (increasing) trend over Asia. A positive trend in atmospheric heating due to aerosols in model simulations is consistent with model simulated trends in AOD (positive) and SSA (negative). These results on model-observations comparison need to be taken into account while examining the projected/expected future climate impacts due to aerosols, and potential value of various mitigation measures, in particular on regional and decadal climate change in Asia which is largely uncertain.

* Corresponding author at: Physical Research Laboratory, Ahmedabad, India.
E-mail addresses: ram@prl.res.in, srikanthan.ramachandran@iass-potsdam.de (S. Ramachandran).

https://doi.org/10.1016/j.scitotenv.2021.150756

Main finding: Our analysis of satellite and ground-based observations, and simulations from climate models in CMIP6 experiment with state-of-the-art treatment of aerosol chemistry, physics and meteorology reveal large difference in model calculations, and most models are not able to capture the recent observed trends in aerosol optical depth and single scattering albedo over Asia during 2000-2018.

1. Introduction

The regional distributions of both aerosol direct radiative and indirect radiative effects on climate are highly heterogeneous across the regions due to substantial regional variations in concentrations of various aerosols (IPCC, 2013). On the global scale, aerosol emissions cause a net negative radiative forcing (cooling) on climate, and it is thought to have offset almost a third of the warming due to increases in greenhouse gases (IPCC, 2013). However, aerosol direct effect is uncertain by a factor of three, and the uncertainties over the aerosol indirect effects are even larger (IPCC, 2013). Furthermore, light-absorbing aerosols such as black carbon (BC), brown carbon (BrC) and dust deposited on snow and ice decrease the surface albedo and as a result generate an additional positive radiative forcing. In the last few decades, Asia has been the largest source of anthropogenic aerosols and their precursor gases (Zhang et al., 2012; Li et al., 2016). The large and dense population, rapid industrial and urban growth, and emissions of huge amounts of air pollutants and greenhouse gases, and potential impacts of climate change on its sensitive ecosystems (e.g., freshwater, biodiversity, agriculture), human health and large societal costs within and extended cost beyond Asia make Asia extremely vulnerable to climate change risks (IPCC, 2013; IPCC, 2021). Because of these sensitive issues of regional and global importance a proper understanding of how the Asian aerosols impact climate from local to regional to global scales becomes a critical issue (Ramanathan et al., 2007; Samset et al., 2019).

The economic activities and air pollution regulations in the last decade have significantly changed aerosol emissions and atmospheric loading in Asia. Satellite observations have documented changes in the geographical distributions of aerosols over Asia (Myhre et al., 2017; Ramachandran et al., 2020). The composition, content and spatial patterns of aerosols are changing over Asia mainly because of changes in emissions of anthropogenic aerosols and their precursors (Samset et al., 2019; Ramachandran et al., 2020). Whereas, in general, there has been a decrease in aerosol emissions worldwide recently, aerosol pollution has been increasing over South Asia and decreasing significantly over East Asia, creating a so-called aerosol dipole between South Asia and East Asia (Samset et al., 2019; Ramachandran et al., 2020). The emissions of air pollutants over China have been declining since stringent air pollution control measures were enforced in China starting from the 2008 summer Olympics in Beijing (Ramachandran et al., 2020). Subsequently, the aerosol optical depth (AOD) has been sharply decreasing over East Asia (Ramachandran et al., 2020) as a result of continued reduction in emissions of anthropogenic primary aerosols and aerosol precursor gases from China. The aerosol-radiation-cloud radiative forcing arising out of the current evolving aerosol dipole pattern in Asia will be different from that of the observed aerosol characteristics in the late 20th century, and it may induce regional-scale atmospheric responses and anomalies with wide-ranging impacts on climate, clouds, chemistry, and monsoon extending well beyond the aerosol source regions in Asia (Zhao et al., 2019; Samset et al., 2019). The South and East Asian regions are specifically vulnerable owing to the significant seasonal variations in precipitation (e.g., monsoon) on which their agriculture and economy are crucially dependent (Samset et al., 2019; IPCC, 2013).

The projected climate impact of various aerosol effects in the international and national climate assessments, such as by the Intergovernmental Panel on Climate Change (IPCC), depends extensively on the results from multi-model climate simulations (Katarzyna et al., 2020). The IPCC, 2013 report featured the results from the coordinated Coupled Model Intercomparison Project Phase 5 (CMIP5) (IPCC, 2013). The results from CMIP phase 6 (CMIP6) are used in the IPCC 6th Assessment Report (AR6). Thus, it is imperative and pertinent to examine the simulations by the current state-of-the-art climate models under CMIP6 in order to discern the ability of these models to capture accurately the features of the Asian aerosol dipole. Further, the multi-model analysis conducted to examine the present trends in aerosols will be useful to evaluate the future climate projections of these model simulations. Here, we make use of the results from the multi-model simulations from CMIP6 and their ensemble mean (Table 1), for the first time, to analyze the trends in aerosol optical depth (AOD), and single scattering albedo (SSA) over South Asia and East Asia during the last 2-decades (2002–2018) and compare these with results from satellite data and ground-based observations. Trends in AOD from CMIP6 models have been reported recently – between 2006 and 2014 (Wang et al., 2021), and between 2001 and 2017 (Cherian and Quaas, 2020), however, trends in SSA have not been reported yet. SSA, a measure of aerosol absorption, and its trends are more crucial for determining the aerosol radiative effects accurately.

Table 1
List of the models contributing to the CMIP6 experiments that are used in this study, the modelling centers leading the modelling efforts, atmospheric model resolution, and number of ensemble members.

Serial Number	Model Name	Modelling Center/Institute ID/Country	Model resolution (Latitude × Longitude)	Ensembles
1	CanESM5	CCCma/Canada	2.8125° × 2.8125°	10
2	CNRM-ESM2-1	CNRM-CERFACS, France	1.4° × 1.4°	3
3	CESM2	NCAR/USA	1.25° × 0.9375°	3
4	CESM2-WACCM	NCAR/USA	1.25° × 0.9375°	3
5	GFDL-CM4/ESM-4	NOAA-GFDL/USA	1.25° × 1.0°	1
6	GISS-E2-1-G	NASA-GISS/USA	2.5° × 2.0°	5
7	HadGEM3-GC31-LL	MOHC/UK	1.875° × 1.25°	4
8	UKESM1-0-LL	MOHC/UK	1.875° × 1.25°	4
9	IPSL-CM6A-LR	IPSL/France	2.5° × 1.259°	3
10	MIROC-ES2L/MIROC6	MIROC/Japan	2.8° × 2.8°	3
11	MPI-ESM1-2-LR	MPI-M/Germany	1.875° × 1.875°	5
12	MRI-ESM2-0	MRI/Japan	1.125° × 1.125°	5
13	NorESM2-LM	NCC/Norway	2.5° × 1.875°	1

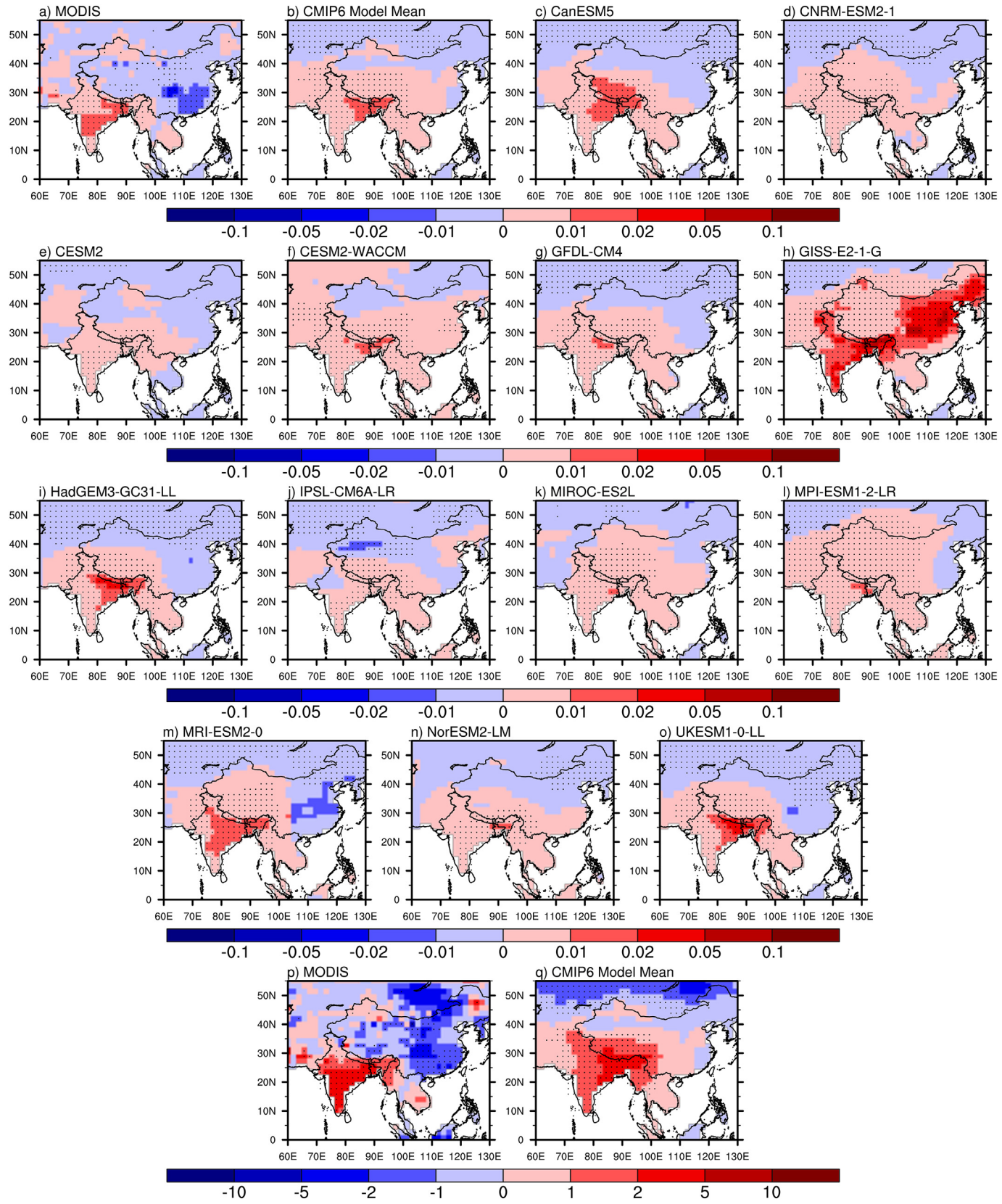

Fig. 1. Trends in aerosol optical depth (AOD) over South Asia and East Asia: Linear trends between 2002 and 2018 for the Asian region (year^{-1}) for AOD at 0.55 μm (a) in satellite observations (MODIS), (b) multi-model mean of CMIP6 model simulations, and the trends obtained for each model in CMIP6, in particular for (c) CanESM5, (d) CMRM-ESM2-1, (e) CESM2, (f) CESM2-WACCM, (g) GFDL-CM4, (h) GISS-E2-1-G, (i) HadGEM3-GC31-LL, (j) IPSl-CM6A-lR, (k) MIROC-ES2L, (l) MPI-ESM1-2-LR, (m) MRI-ESM2-0, (n) NorESM2-LM and (o) UKESM1-0-LL (Table 1). Relative (percent) trends between 2002 and 2018 for the Asian region (% year^{-1}) for AOD at 0.55 μm (p) in satellite observations (MODIS) and (q) multi-model mean of CMIP6 model simulations (Table 1), Black dots correspond to points where the trend is significant at the 95% confidence level.

2. Data, analysis and methods

2.1. Models

The CMIP (Coupled Model Intercomparison Project) is designed to better understand the past, present and future climate change due to natural and anthropogenic radiative forcing using multi-model simulations (Eyring et al., 2016). Simulation results from 13 models from the CMIP Phase 6 (CMIP6) (https://esgf-node.llnl.gov/search/cmip6/) (Eyring et al., 2016, Table 1) are utilized in this study. Details of the models contributing to the CMIP6 experiments that are used in this study are provided in Table 1.

2.2. Simulations

Specific CMIP6 experiments are designed to explore the climate change arising from the changes in aerosols, greenhouse gases, and natural forcings. In this study, CMIP6 "historical" simulations are used for the analysis. The CMIP6 "historical" simulations run until 2014 are complemented with a "ScenarioMIP" simulation (Eyring et al., 2016; O'Neill et al., 2016) for the 2015 to 2018 period. The selected scenario is the "Shared Socioeconomic Pathways" (SSP245) that follows SSP2 (middle of the road) pathway, and reaches in 2100 a global mean forcing of 4.5 Wm^{-2} relative to pre-industrial time (Eyring et al., 2016; O'Neill et al., 2016). Effective radiative forcing (ERF), due to aerosol-

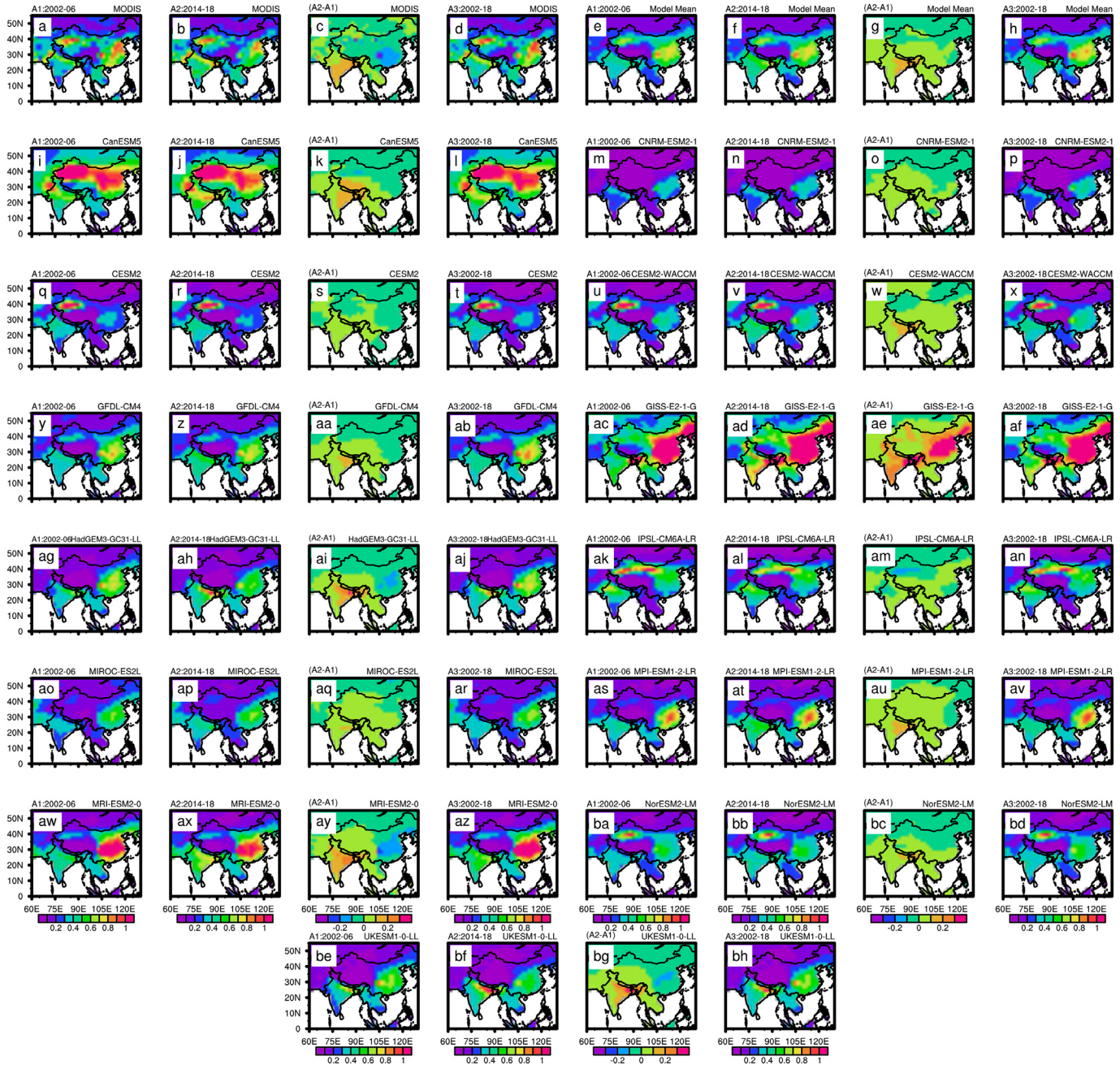

Fig. 2. Aerosol optical depth over Asia – observations and model simulations: MODIS satellite retrieved aerosol optical depth (AOD) averaged for 2002–2006 (A1), 2014–2018 (A2), their difference (A2-A1), and average for 2002–2018 (A3) (a–d) in comparison with multi-model (Table 1) mean (e–h), and with individual models - CanESM5 (i–l), CNRM-ESM2-1 (m–p), CESM2 (q–t), CESM2-WACCM (u-x), GFDL-CM4 (y–ab), GISS-E2-1-G (ac–af), and HadGEM3-GC3-L1 (ag–aj), IPSL-CM6A-LR (ak–an), MIROC-ES2L (ao–ar), MPI-EMS1-2-LR (as–av), MRI-ESM2-0 (aw–az), NorESM2-LM (ba–bd), and UKESM1-0-L1 (be–bh). Black dots correspond to points where the trend is significant at the 95% confidence level.

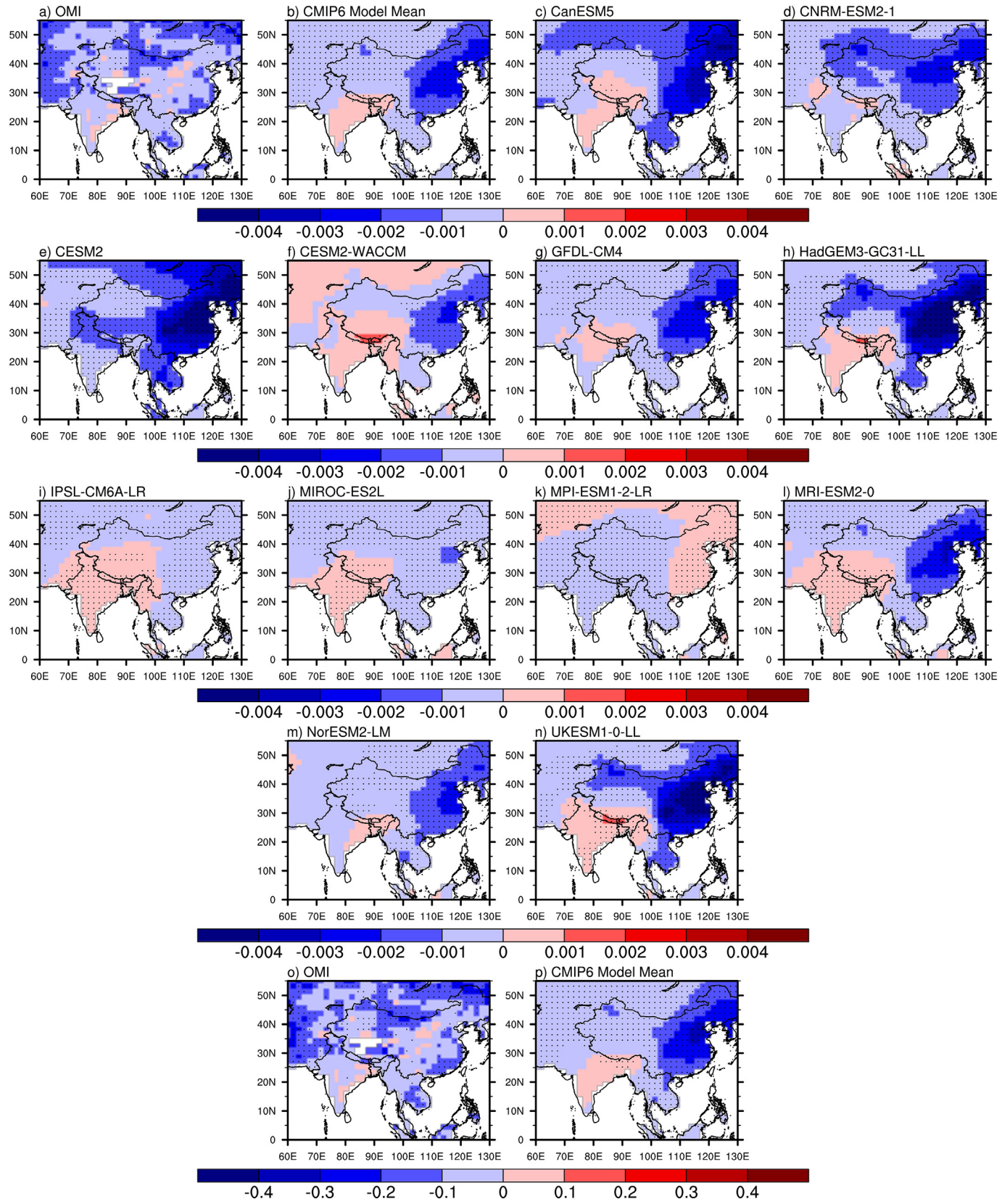

Fig. 3. Trends in single scattering albedo (SSA) over South and East Asia: Linear trends between 2005 and 2018 for the Asian region (year^{-1}) for SSA (a) in satellite observations (OMI), (b) multi-model mean of CMIP6 model simulations, and in each CMIP6 model the outputs of which are used in the study, namely, (c) CanESM5, (d) CMRM-ESM2-1, (e) CESM2, (f) CESM2-WACCM, (g) GFDL-CM4, (h) HadGEM3-GC31-LL, (i) IPSl-CM6A-lR, (j) MIROC-ES2L, (k) MPI-ESM1-2-LR, (l) MRI-ESM2-0, (m) NorESM2-LM and (n) UKESM1-0-LL (Table 1). Relative (percent) trends between 2005 and 2018 for the Asian region (% year^{-1}) for SSA (o) in satellite observations (OMI), and (p) multi-model mean of CMIP6 model simulations. OMI SSA corresponds to 0.388 μm and model SSA corresponds to 0.55 μm (see text for more details). Black dots correspond to points where the trend is significant at the 95% confidence level.

radiation interactions takes into account the rapid adjustments caused by aerosol radiative effects on the surface energy budget (*aerosol direct effect*), the atmospheric profile and cloudiness (*semi-direct effect*), and therefore, it signifies the radiative forcing caused by aerosol direct effect and the semi-direct effect (IPCC, 2013). The model simulated ERF and observed aerosol radiative forcing (ARF) of the atmosphere (ARF_{ATM}) are not directly comparable as the ERF also includes semi-direct effect. The "piClim-control" and "piClim-histaer" simulations are part of the CMIP6 Radiative Forcing Model Intercomparison Project (RFMIP; https://rfmip.leeds.ac.uk/rfmip-erf/) to specifically address the ERF across climate models. The "piClim-control" run uses the boundary conditions fixed at pre-industrial (1850) levels, and serves as the baseline for ERF calculations. The "piClim-histaer" experiment uses time varying emissions of aerosol precursors, but keeping all other boundary conditions fixed at pre-industrial levels. The "piClim-histaer" run is available only from three CMIP6 models (CanESM5, GFDL-CM4 and MIROC6) for the period 2002–2018 and are used for the analysis. ERF within the atmosphere corresponding to the particular year 2014 (present day scenario) (Eyring et al., 2016) are available from CMIP6 simulations which are used in the study for comparison.

Community Emissions Data System (CEDS) inventory for the period from 1850 to 2014 is used in CMIP6 models for historical runs (Hoesly et al., 2018). The future emission projections are used for CMIP6 simulations from 2015 to 2100 (Gidden et al., 2019). Nine emission sectors (agriculture, aircraft, energy, industry, international shipping, residential and commercial, solvent production and application, transportation, and waste) are included. For India, there are increases in anthropogenic emission of sulfur dioxide (SO_2), BC and organic carbon (OC) from 2002 to 2018. For China, emissions were used based on values from Zheng et al. (2018). China's air pollution mitigation measures have yielded reductions of 9.5 Tg of SO_2, 0.3 Tg of BC, and 0.3 Tg of OC from the industrial sector in 2017 compared to their levels in 2010 (Zheng et al., 2018). The AOD and SSA simulated by CMIP6 models (Table 1) at 0.55 μm for 2001–2018 period are used in the study.

2.3. Measurements

The annual mean MODIS AOD was calculated from the daily mean AOD (corresponding to 0.55 μm) from MODIS Daily L3 Global 1 Degree datasets acquired from the Level-1 and Atmosphere Archive and Distribution System (LAADS) (https://ladsweb.modaps.eosdis.nasa.gov/archive/allData/61/MOD08_D3/). The uncertainty in MODIS AOD is ± 0.05 ± 0.15AOD (Levy et al., 2013). The monthly data of OMI (https://disc.gsfc.nasa.gov/datasets/OMAERO_003/summary) SSA was created using the first 23 clean rows of OMI Level-2 product (out of total 60 rows) that are free of row anomaly (Torres et al., 2018) throughout the OMI operation period. The OMI SSA at 0.388 μm is used because retrievals at the other wavelengths in the OMAERUV dataset are not directly derived from the measurements, but converted from 0.388 μm retrievals assuming a spectral dependence model depending upon the

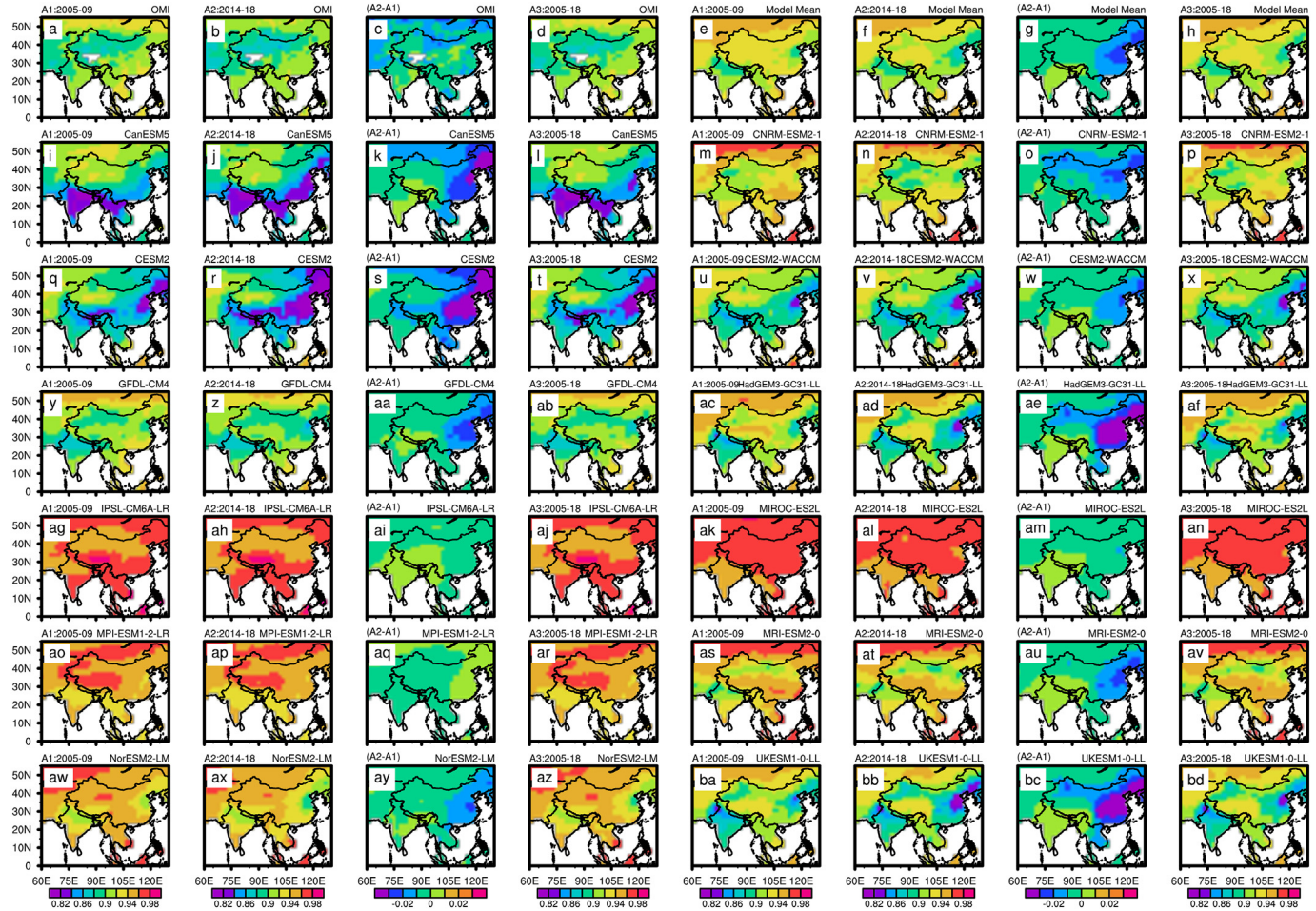

Fig. 4. Aerosol single scattering albedo over Asia – observations and model simulations: OMI satellite retrieved single scattering albedo (SSA) averaged for 2005–2009 (A1), 2014–2018 (A2), the difference between the two periods (A2 and A1), average for 2005–2018 (A3), and linear trends during 2005–2018 (a–d) in comparison with the multi-model (Table 1) mean (e–h), and for individual models - CanESM5 (i–l), CNRM-ESM2-1 (m–p), CESM2 (q–t), CESM2-WACCM (u–x), GFDL-CM4 (y–ab), HadGEM3-GC3-L1 (ac–af), IPSL-CM6A-LR (ag–aj), MIROC-ES2L (ak–an), MPI-ESM1-2-LR (ao–ar), MRI-ESM2-0 (as–av), NorESM2-LM (aw–az), and UKESM1-0-L1 (ba–bd). OMI SSA corresponds to 0.388 μm and model SSA corresponds to 0.55 μm (see text for more details). Black dots correspond to points where the trend is significant at the 95% confidence level.

chosen aerosol model. Due to a few inherent uncertainties in the assumed spectral dependence, which might not represent all aerosol types/conditions globally, it has been recommended to use the 0.388 μm SSA dataset (Torres et al., 2018). The OMI observations, since the middle of 2007, have been affected by a possible external obstruction that perturbs both the measured solar flux and Earth radiance. This obstruction, which affects the quality of radiance at all wavelengths for a particular viewing direction, is referred to as a "row anomaly" since the viewing geometry is associated with the row numbers on the charge-coupled device detectors (Torres et al., 2018). The row anomaly issue was detected initially for a few rows which, over the period of operation, expanded to other rows in 2008 and later. Currently, about half of the total 60 rows (viewing positions) across the track are identified and flagged as affected by row anomaly for which no physical retrievals are being performed. Due to the row anomaly issue and some scan-related bias in the OMI SSA retrievals (Torres et al., 2018), we have utilized the level-2 OMAERUV product for SSA derived using only the first 23 rows that are unaffected by the row anomaly throughout the OMI operation for comparison. SSA derived using viewing positions 1–30, and 31–60 were found to agree over regions dominated by carbonaceous or sulfate particles (Torres et al., 2018). The Level-2 retrievals are aggregated on to each 0.5° × 0.5° grid. Note that only best quality retrievals (Quality Flag = 0) of SSA at 0.388 μm are included in this analysis. In a global analysis of collocated retrievals, Jethva et al. (2014) reported that ca. 70% of OMI-AERONET SSA (at 0.44 μm) matchups agreed within the absolute difference of ±0.05 for all aerosol types. In case of Aerosol Robotic Network (AERONET) data, annual means of AOD and SSA were calculated from the quality assured (level 2, version 3, cloud screened) daily AOD (retrieved from direct Sun algorithm), and SSA (retrieved from solar almucantar inversion algorithm) at 0.55 μm measured with ground-based Cimel Sun/sky radiometers (https://aeronet.gsfc.nasa.gov/) (Holben et al., 2001) for 2002 to 2018 over Kanpur and Beijing, the two sites with the longest time series of level 2 data in Asia. The uncertainty in AERONET AOD is less than ±0.01 at 0.55 μm, and SSA is uncertain by ±0.03 when the AOD at 0.44 μm is >0.2 (Holben et al., 2001). Observations suggest that the spectral variation in SSA in the wavelength region of 0.388–0.55 μm is not significant (Ramachandran et al., 2015 and references therein). Thus, a comparison of OMI (0.388 μm) and model derived SSA (0.55 μm) is not potentially expected to contribute any significant differences in trends due to the above as well as due to the fact that OMI SSA at 0.388 μm is more robust than the OMI SSA derived at 0.55 μm.

2.4. Trend analysis

In the current study the least squares linear trend method is used to estimate the trends in aerosol parameters. The statistical significance of the trends is computed using a two-tailed student *t*-test. The statistical significance is calculated using the regression line information on a grid-by-grid basis using monthly data for the same time period from satellite and models from 2002 to 2018 for AOD, and from 2005 to 2018 for SSA (with no missing time periods). The least squares linear regression method is a simple and robust method, and is a widely used method to estimate the trends in the time-dependent geographical and environmental variables. The method is less sensitive to gaps in the time series of data, and further, it is quite appropriate when the uncertainty in data is constant (i.e., Gaussian white noise) so that regression can be obtained by allocating a weight of unity (i.e., assigning the same precision) to each parameter (Ramachandran et al., 2020).

3. Results and discussion

3.1. Aerosol optical depth

The CMIP6 multi-model mean shows an increasing trend in AOD during 2002–2018 over almost entire South Asia, East Asia and southeast Asia, with trends statistically significant at 95% confidence level (CL) over entire South Asia, southwestern China and northwestern part of southeast Asia, and not significant over East Asia. There are negative trends in AOD over northern and eastern China but they are not

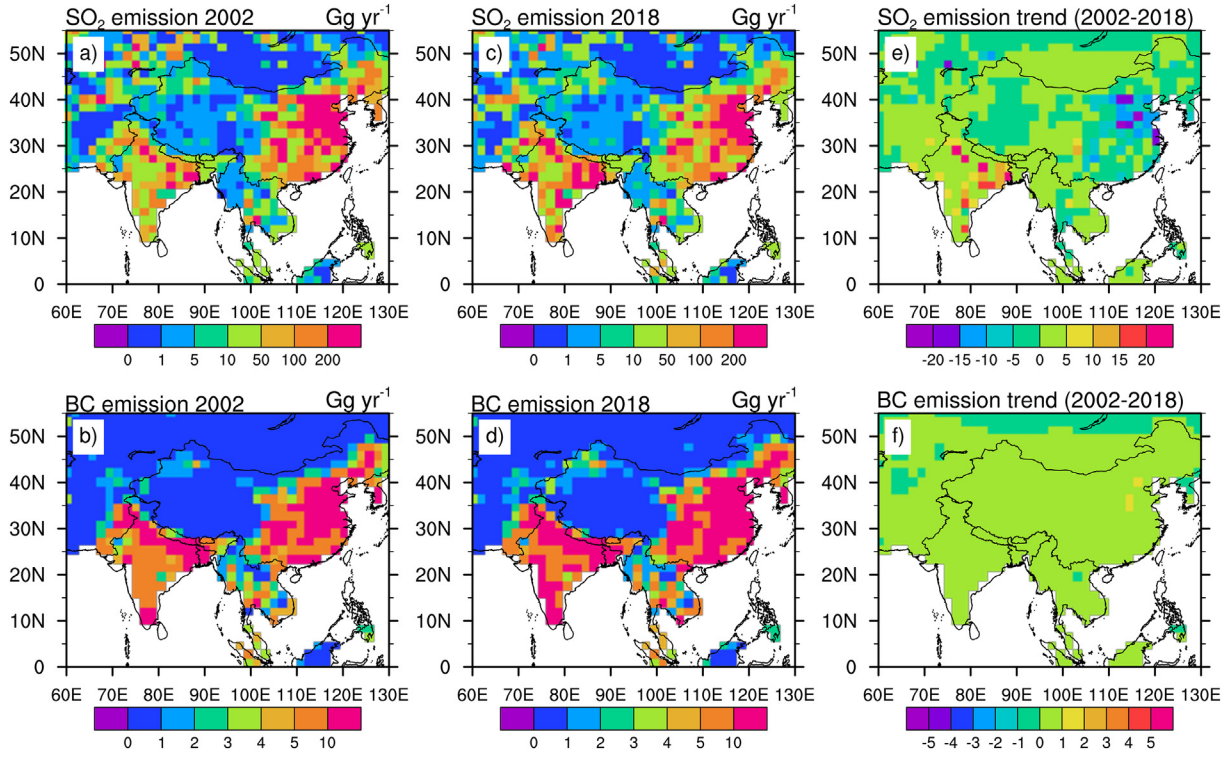

Fig. 5. Aerosol emissions and their evolution over Asia: Sulfur dioxide (SO_2) and black carbon (BC) emissions (in Gg per year) over Asia for 2002 (a, b), 2018 (c, d) and their respective absolute trends (e, f).

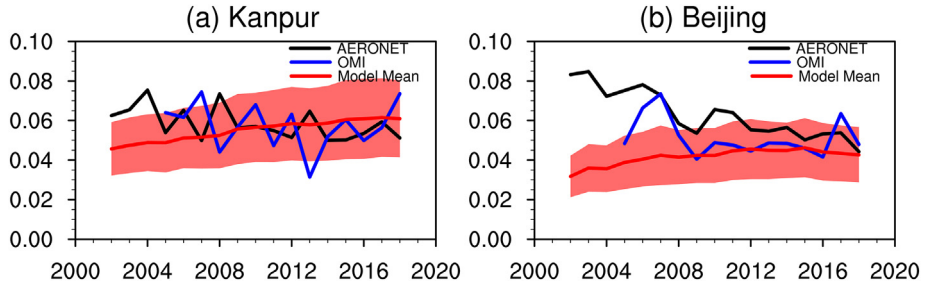

Fig. 6. Annual trends in annual mean absorption aerosol optical depth (AAOD) over (a) Kanpur and (b) Beijing during 2002–2018 from ground-based observations (AERONET), satellites (AOD from MODIS and SSA from OMI), and CMIP6 multi-model mean (thick red line). The satellite and model results correspond to the grids in which the study locations – Kanpur (26.5°N, 80.2°E) and Beijing (39.9°N, 116.4°E) - are located. The shaded region indicates the 5% to 95% confidence intervals by the CMIP6 models (Table 1, Figs. 1–4). (For interpretation of the references to colour in this figure legend, the reader is directed to the web version of this article.)

statistically significant (Fig. 1). In contrast, satellite observations of AOD clearly show a regional-scale aerosol dipole between South Asia (positive) and East Asia (negative). Although the multi-model mean fails to capture the trends in East Asia, individual realizations of six models (CanESM5, CESM2, GDL-CM4, HadGEM3-GC3-1-LL, UKESM1-0-LL and MRI-ESM2-0) are able to simulate a weaker negative trend (not statistically significant) over northern parts of East Asia (Figs. 1, 2). Most models simulate high AODs over both South and East Asia instead of a

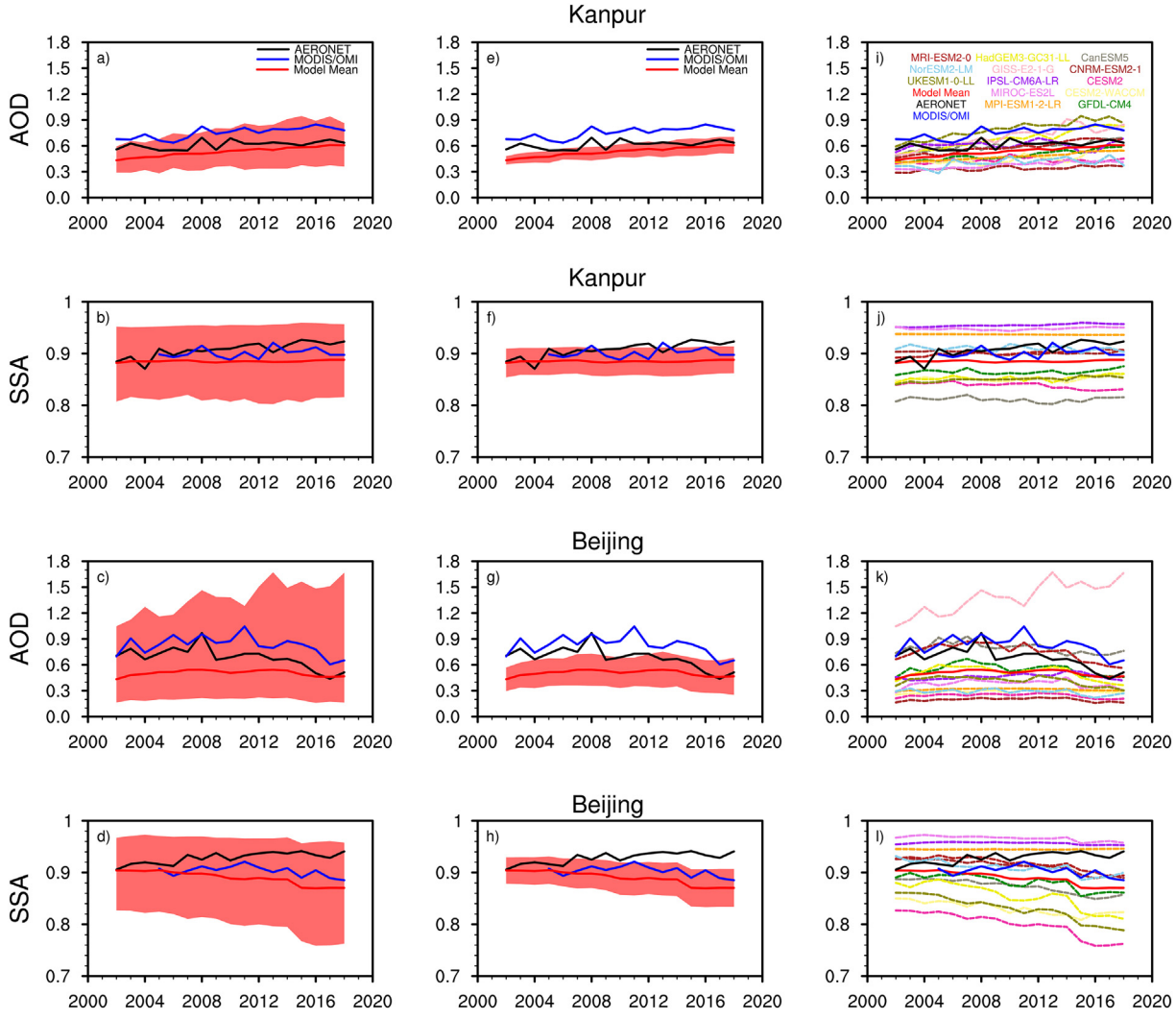

Fig. 7. Aerosol optical properties over Kanpur and Beijing during 2002–2018: Time series of annual mean AOD (a, c) and SSA (b, d) over Kanpur and Beijing, respectively, from ground-based observations (AERONET), satellites (AOD from MODIS and SSA from OMI), and the CMIP6 multi-model mean. In all the figures ((a)-(l)) ground-based observations from AERONET are drawn as black line, satellite data on AOD from MODIS and SSA from OMI are shown in blue line, and the CMIP6 multi-model mean are given in red line. The satellite and model results correspond to grids where the study locations – Kanpur (26.5°N, 80.2°E) and Beijing (39.9°N, 116.4°E) are located. The shaded region in (a), (b), (c) and (d) corresponds to the maximum and minimum values among the values simulated by the thirteen CMIP6 models (Table 1). AODs from MODIS, AERONET and CMIP6 models correspond to 0.55 μm, while SSA from OMI corresponds to 0.388 μm and that of AERONET and CMIP6 models correspond to 0.55 μm respectively. The shaded region in (e), (f), (g) and (h) indicate the 5% to 95% confidence intervals by the CMIP6 models (Table 1, Figs. 1–4). The simulated values by individual CMIP6 models are shown as thin colored lines in (i), (j), (k) and (l). (For interpretation of the references to colour in this figure legend, the reader is directed to the web version of this article.)

dipole, and the high AODs across the Indo-Gangetic Plain (IGP), a profound feature of aerosol loading over Asia is missing in most model simulations (Fig. 2). Furthermore, the magnitude of simulated AODs across models differ significantly – AODs are lower in CNRM-ESM2-1 and CESM2 simulations with respect to the model mean and observations, whereas the AODs are a factor of 2-higher in CanESM5 and GISS-E2-1-G simulations (Fig. 2) compared to the above models. The positive trends in AOD from satellite observations are statistically significant over India, Bangladesh and northwestern Myanmar whereas the negative trends are statistically significant over most of China (Fig. 1). The positive trend in model AOD is higher (>0.01 AOD per year) over eastern IGP in South Asia while in observations a higher positive trend is seen over south and central India, and a small part of the eastern IGP (Fig. 1). In the satellite observations a statistically significant higher negative trend (−0.01 to −0.02 per year) in AOD is seen over eastern China the region over which the model-mean has a positive trend, which, however, is not statistically significant. Over the rest of Asia the increase or decrease in AOD is ≤0.01 or ≥−0.01 per year. An analysis of seasonal trends in observed AODs (satellite and ground-based) revealed that the positive trends in annual mean AOD and SSA over the IGP in South Asia are controlled by their trends during post-monsoon and winter seasons (Ramachandran et al., 2020), which are dominated by anthropogenic aerosol emissions. This result corroborates well an observational (satellite and ground-based) analysis which found ca. 0.02 per year increase in AOD in the post-monsoon and winter seasons over the IGP during 2002–2016 (Jethva et al., 2019; Ramachandran et al., 2020), which was associated with a positive trend in emissions from agro-residue burning in addition to the increase in emissions from fossil fuel combustion. Thus, it is clear that the positive trend in AOD over South Asia in observations and model simulations is due to the increasing emissions from fossil fuel and biomass burning sources.

3.2. Single scattering albedo

In case of SSA, the multi-model mean exhibits a negative trend (statistically significant) during 2005–2018 over East Asia and generally positive trend (statistically insignificant) over much of South Asia (Fig. 3). The SSA derived from the satellite observation (OMI) shows negative trends (statistically insignificant) over most of East Asia and South Asia (except a narrow strip of east coast of India and eastern IGP including Bangladesh). The rate of decrease in SSA, however, is an order of magnitude smaller than that of AOD. It may be difficult to envisage a comparison of absolute (linear) trends in the 'unit' of AOD and SSA which is the focus of the study and not in terms of relative (percentile) trends, as the amount of variation will depend on the 'unit' itself - in this case AOD naturally has a larger range than SSA. We calculated the relative (percentile) trends (% year^{-1}) of AOD and SSA by dividing the slope of the trend with the median value of AOD (obtained for the time period 2002–2018) (Fig. 1p, q) and SSA (obtained for the time period 2005–2018) (Fig. 3o, p). The analysis reveals that even the relative (percentile) trends for AOD have a larger range than SSA, and are at least 5–8% higher for AOD than the trends in SSA, similar to their respective linear trends (Figs. 1a, b, 3a, b). The rate of decrease in model-mean SSA is significantly higher, at least by 3-times, over the North China Plain (NCP) than the rest of Asia. A decrease in SSA suggests an increase in proportion of aerosol absorption (either proportion of scattering aerosols, e.g., sulfate has decreased and/or that of absorbing aerosols, e.g., BC has increased). As mentioned earlier, emissions of SO_2, BC, and other air pollutants have been reduced more rapidly over China than India (Li et al., 2017; Zheng et al., 2018), which however, have not resulted in an increase in SSA as evident from the satellite observations and model simulations (Figs. 3, 4). SSA values also exhibit a significant range across the CMIP6 models – the aerosols are considered more

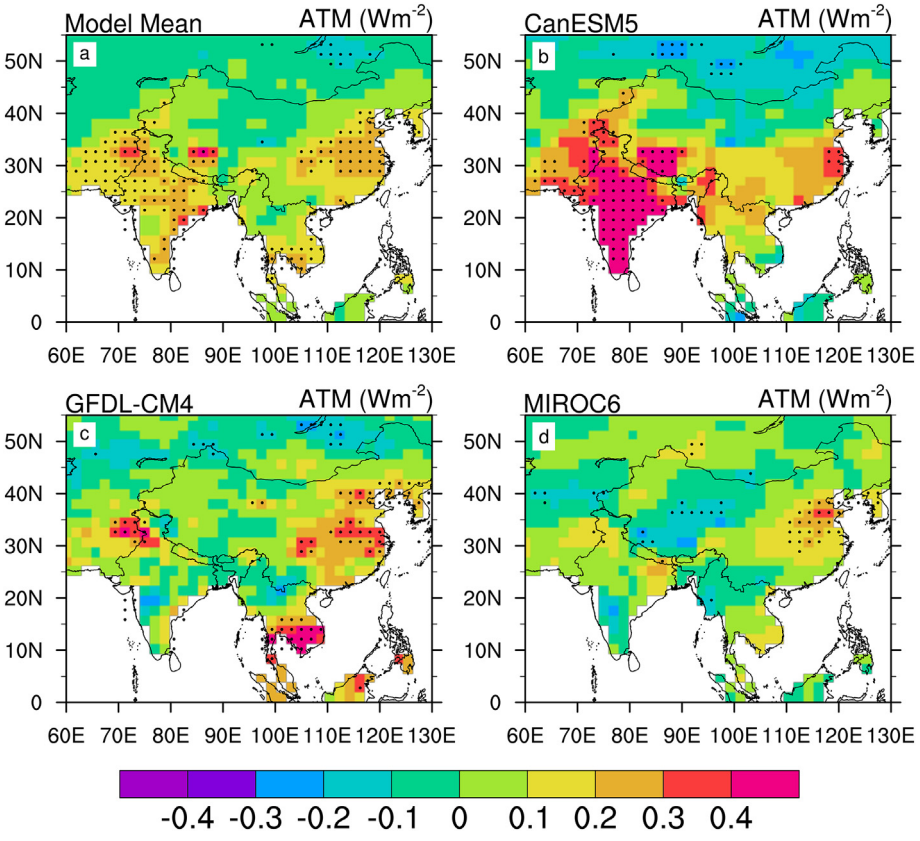

Fig. 8. Trends in aerosol radiative forcing over South and East Asia: Linear trend of aerosol-induced effective radiative forcing (ERF, Wm^{-2}) in the atmosphere (ATM) (ERF$_{ATM}$) (= ERF at the top of the atmosphere (TOA) – ERF at the surface (SFC)) over the Asian region (year^{-1}) between 2002 and 2018 in (a) multi-model mean of CMIP6 model simulations, (b) CanESM5, (c) GFDL-CM4 and (d) MIROC6 (Table 1). Black dots correspond to points where the trend is significant at the 95% confidence level.

absorbing if 0.85 ≤ SSA < 0.90 (CanESM5), moderately absorbing if 0.90 ≤ SSA < 0.95 (GFDL-CM4), and less absorbing if SSA >0.95 (IPSL-CM6A-LR, MIROC-ES2L, MPI-ESM1-2-LR) (Figs. 3, 4).

The reduction in emissions of SO_2, BC and other air pollutants has been more rapid in China than India due to highly successful aggressive emission control policies in China (Li et al., 2017; Zheng et al., 2018; Kanaya et al., 2020). Chinese emissions of both SO_2 and BC have decreased (Zheng et al., 2018; Kurokawa and Ohara, 2020; Kanaya et al., 2020); however, with significantly different rates – SO_2 by 62% and BC by 28% during 2010–17 (Zheng et al., 2018). The decrease in SO_2 emissions is seen more clearly than BC emissions (which have changed only slightly during the last 2-decades) over China (Fig. 5). A significant reduction in SO_2 as compared to little changes in BC (and OC), with decrease in both emissions from 2015 to 2017 being slower in CMIP6 models than observation-based changes over China (Wang et al., 2021) result in an increase in aerosol absorption (Fig. 6) leading to stronger negative SSA trends in the models (Figs. 3, 4). In contrast, in India the emissions of $PM_{2.5}$ and BC have increased concurrently with increase in the coal and heavy oil consumption in thermal power plants and industries, and diesel in transport sector (Sadavarte and Venkataraman, 2014; Kurokawa and Ohara, 2020). The increase in $PM_{2.5}$ and SO_2 emissions from the industrial sector in India was ~2.5 times larger than the increase in fuel consumption during 1996–2015, which was attributed to the growth in process emissions resulting from an increase in production activity (Sadavarte and Venkataraman, 2014). In the transport sector, the increase in these emissions was smaller than the corresponding increase in fuel consumption, owing to the implementation of emissions and fuel quality norms (Sadavarte and Venkataraman, 2014). The biomass burning amounts over India were nearly constant during the last decades as compared to China where biomass use has been decreasing (Sadavarte and Venkataraman, 2014).

The CMIP6 models' failure to capture the magnitude, regional distribution, and the trends in AOD and SSA is re-emphasized here in a comparison with ground-based observations from two AERONET sites with longest records in South Asia and East Asia (Fig. 7) - Kanpur (26.5°N, 80.2°E, 123 m above mean sea level (asl)) located in central IGP in South Asia and Beijing (39.9°N, 116.4°E, 92 m asl) located in NCP in East Asia (Fig. 7). Kanpur is an industrialized, densely populated (with ca. 3 million inhabitants in 2011) and a highly polluted city. It is located

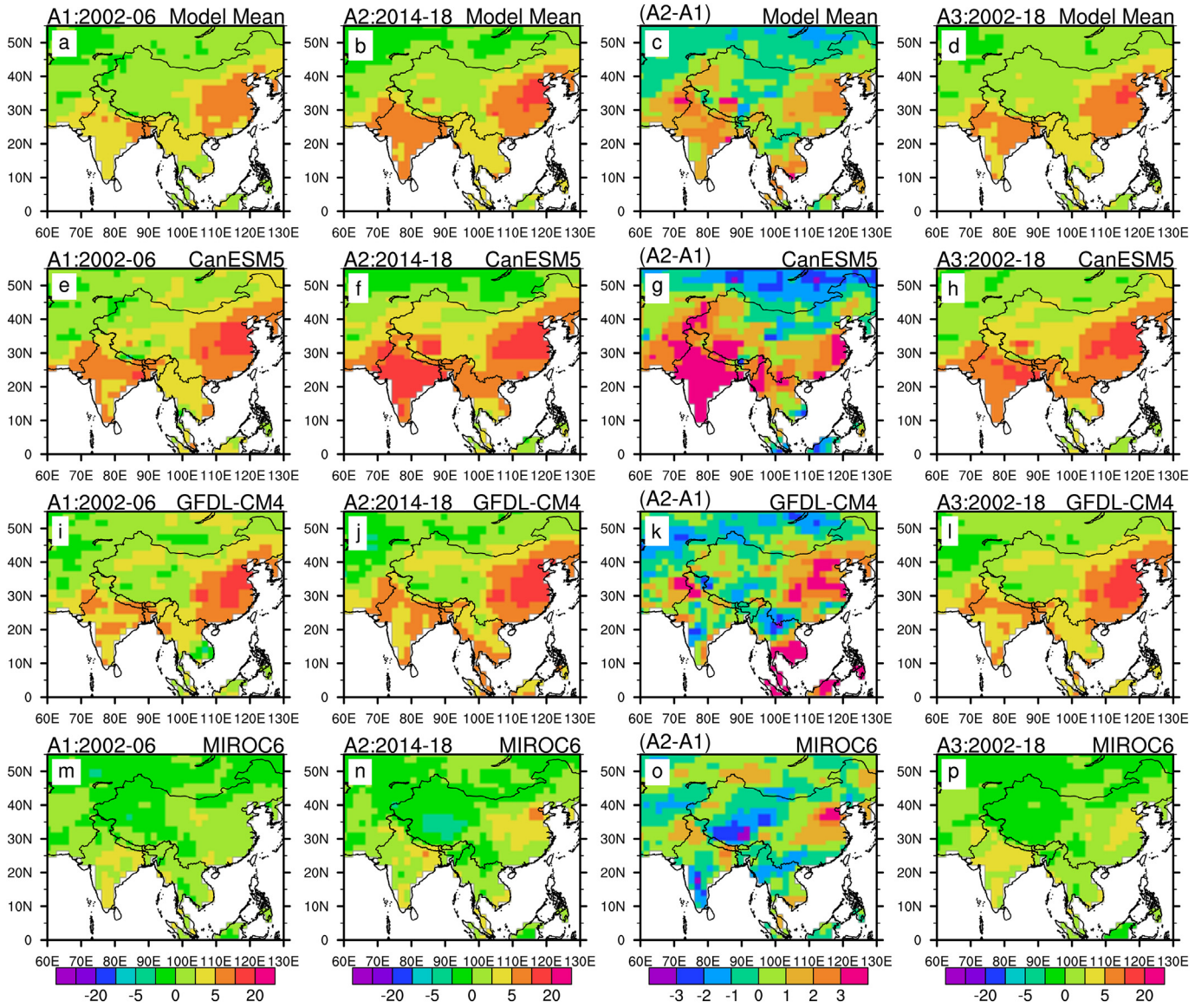

Fig. 9. Aerosol radiative forcing over Asia – model-mean and models: Multi-model mean aerosol-induced effective radiative forcing in the atmosphere (ERF_{ATM}, Wm^{-2}) in the atmosphere (ATM) averaged for 2002–2006 (A1) (a), and 2014–2018 (A2) (b), the difference between the two time periods ((2014–2018) – (2002–2006)) (c), average for 2002–2018 (A3) (d). Same as above for results obtained from model simulations of CanESM5 (e-h), GFDL-CM4 (i-l) and MIROC6 (m-p).

ca. 500 km to the southeast of the megacity New Delhi (ca. 19 million population). Beijing, another megacity in Asia (with 21 million population), is situated in the heavily polluted and heavily industrialized NCP. Aerosol characteristics over both Kanpur and Beijing are quite similar as they are urban centers located in generally similar settings. The heavy aerosol pollution over these locations arises mainly from biomass burning emissions and fossil fuel combustion during all seasons with different seasonal contributions of some specific sources (Eck et al., 2010; Ramachandran et al., 2020). On a seasonal scale during the spring season (March-April-May) dust from nearby deserts and arid regions contribute to the aerosol loading over both IGP and NCP. Emissions from biomass burning in South Asia, i.e., forest fires and agro-residue burning during pre-monsoon season and agro-residue burning during post-monsoon in addition to biomass use for residential activities which occurs throughout the year, affects heavily the aerosol loading in South Asia (Ramachandran et al., 2015; Jethva et al., 2019; Ramachandran et al., 2020). Thus, both locations are strongly influenced by regional emissions as well as their own local sources. The ground-based observations of AOD and SSA over Kanpur and Beijing exhibit remarkably different features among them in comparison with satellite and model results, despite the satellite and model results correspond to grids where the study locations – Kanpur (26.5°N, 80.2°E) and Beijing (39.9°N, 116.4°E) are located. The dipole in aerosol content (AOD) is clearly visible with that of a negative trend in AOD over Beijing and a positive trend over Kanpur (Fig. 7a, c). In contrast, the trend in SSA is the same over both the locations, which is positive in nature suggesting that aerosols have become relatively less absorbing (or more scattering) in the recent times than they were a decade ago (Fig. 7b, d). It is clearly evident that the satellites and models are not able to capture the magnitude of observed (ground-based) AOD and SSA as well (Fig. 7a–d). The ground-based observations of AOD lie between the satellite and models while the SSA values are higher than satellite and models, with the model-mean being the lowest among three different datasets (Fig. 7a–d). The observed AOD and SSA are beyond the bounds of the 5 to 95% confidence level interval (by CMIP6 models) during 2002–2010, and 2010–2018 respectively over Kanpur and Beijing (Fig. 7e–h) as the models exhibit significant differences (Fig. 7i–l). The MODIS AODs show a positive trend over Kanpur and a negative trend over Beijing similar to the ground-based observations. The performance of the models differs in these two locations – model AODs show an increase over Kanpur whereas the models struggle to capture the observed trend, staying more or less same during the last 2-decades over Beijing. More remarkably, the ground-based SSA shows clearly a positive trend in both the locations whereas both the satellite observations and model simulations show a negative trend, more so over Beijing (Fig. 7d). Therefore, aerosol composition and associated optical properties over Asia, in particular aerosol absorption, may not be properly represented in models, as for example, decreases in emissions of SO_2 and BC in CMIP6 models over China are far too slower than observation-based emissions reduction (Wang et al., 2021), and biomass burning aerosols are too absorbing in many current climate models (Brown et al., 2021).

4. Implications and summary

For an accurate and better quantification of direct and indirect radiative effects of aerosols not only the trends but also the magnitude in AOD and SSA are crucial, especially over highly polluted aerosol source region like Asia, because the radiative effects have a linear relation with column aerosol content (AOD) while they exhibit a non-linear relation with composition (SSA) (Ramanathan et al., 2007; IPCC, 2013; Ramachandran et al., 2020). For example, the atmospheric heating due to aerosols will increase by 10% for a 10% increase in AOD and vice versa, whereas the atmospheric heating will increase by >20% when SSA decreases by 10% from 1.00 to 0.90 (Ramachandran et al., 2020). Results from the present study bring out clearly that the CMIP6 models are unable to simulate the recently observed aerosol trends (AOD and SSA), their magnitudes and regional distributions over Asia despite all the models in CMIP6 using the same aerosol emissions (Fig. 5) and initial boundary conditions. An analysis of seasonal trends in observed AOD and SSA over South Asia and East Asia conducted earlier revealed that the changes (increase/decline) in AOD and SSA over the IGP and the NCP during the last two decades occurred primarily due to the increase or decrease in emissions of anthropogenic aerosols and aerosol precursor gases, whereas there was no significant change in atmospheric loading of natural aerosols (dust and sea salt) over these two regions

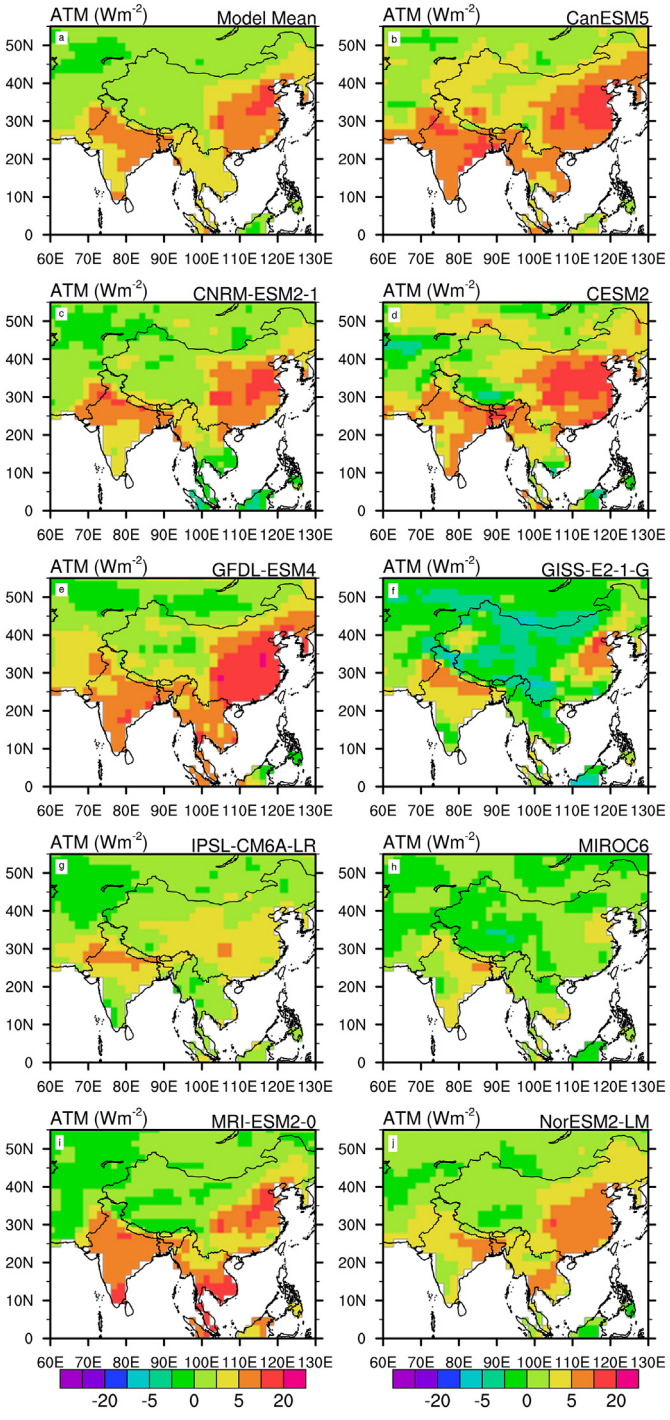

Fig. 10. Aerosol radiative forcing over Asia for 2014: Aerosol-induced effective radiative forcing in the atmosphere (ERF_{ATM}, Wm^{-2}) for the year 2014 simulated by nine CMIP 6 models and their mean – (a) model-mean, (b) CanESM5, (c) CNRM-ESM2-1, (d) CESM2, (e) GFDL-ESM4, (f) GISS-E2-1-G, (g) IPSL-CA6A-LR, (h) MIROC6, (i) MRI-ESM2-0, and (j) NorESM2-LM.

(Ramachandran et al., 2020). The discrepancies in aerosol properties observed between models and measurements were attributed to the lack of/absence of proper aerosol emissions and removal mechanisms in the models over the south Asian region (Ramachandran et al., 2015). However, the present analysis over Asia clearly points to the fact that in addition to discrepancies in emission inventories (not applicable for the CMIP6), representation of aerosol properties, atmospheric transport, and processes such as wet and dry deposition in models could be contributing significantly to the differences between observations and model simulations (e.g., Myhre et al., 2013). The climate responses to the changing aerosol patterns over Asia have become highly uncertain as the climate models are not able to capture the recent trends in aerosol content (AOD) and composition (SSA, AAOD), thus, leading to an uncertainty in the model projected/predicted aerosol effect on monsoon and precipitation. The trends in these two aerosol parameters are the most crucial to estimate the direct and indirect radiative effects of aerosols.

Owing to the changes (decrease/increase) in aerosol content (AOD) and composition (SSA) the aerosol-induced atmospheric heating rate (HR) has decreased considerably in the last two decades over Asia despite a dipole in AOD between South Asia and East Asia (Ramachandran et al., 2020). The decrease in HR is more significant over East Asia (30%) due to decreasing AOD and increasing SSA compared to South Asia (10%) where both AOD and SSA are increasing. The aerosol-induced effective radiative forcing (ERF within the atmosphere (ERF_{ATM})) simulated with three CMIP6 models and their model-mean show a positive trend over Asia (Figs. 8, 9). ERF_{ATM} simulated by nine different CMIP6 models for the year 2014 do not differ significantly (Fig. 10), implying that the trends in ERF_{ATM} if simulated by the other CMIP6 models would also be comparable to the trends obtained from the 3-model mean (shown in Fig. 9). A positive trend in atmospheric heating due to aerosols in model simulations is consistent with the model simulated trends in AOD (positive) and SSA (negative) (Figs. 1, 2). Given the relation of aerosol radiative effects is linear with AOD, and non-linear with SSA, ERF_{ATM} should be lower if we considered the observed trends in AOD (positive) and SSA (negative). Li et al. (2016) report that none of the models were able to account satisfactorily the combination of changes over Asia – weakening of monsoon circulation, decrease in South Asian rainfall versus an increase in southern China's rainfall. These new results on model-observations intercomparison serve as an eye opener which need to be taken into account while examining the projected/expected present and future climate impacts due to aerosols, and the potential value of various mitigation measures, in particular on regional and decadal climate change in Asia which is largely uncertain.

Funding

The IASS is funded by the German Federal Ministry of Education and Research (BMBF) and the Brandenburg State Ministry for Science, Research and Culture (MWFK). SR is an Affiliate Scholar of IASS. R. Cherian acknowledges the funding support by the German Research Foundation (DFG) (project number: 637230).

CRediT authorship contribution statement

SR designed the study in consultation with MR and RC. SR and RC performed the analysis. SR wrote the paper. All authors reviewed and edited the paper.

Data availability

All data used in the manuscript are available publicly: model results at https://esgf-node.llnl.gov/search/cmip6/, MODIS data at https://ladsweb.modaps.eosdis.nasa.gov/archive/allData/61/MOD08_D3/, OMI data at https://disc.gsfc.nasa.gov/datasets/OMAERO_003/summary, and the AERONET data at https://aeronet.gsfc.nasa.gov/.

Declaration of competing interest

The authors declare no conflict of interests.

Acknowledgements

We used data from various publicly available data base. We acknowledge the climate modelling community, PCMDI, and the World Climate Data Centre, Hamburg, Germany for providing the climate model results. We thank the MODIS and OMI mission scientists, associated NASA personnel and data centers for the production and maintenance of the satellite data. We acknowledge the principal investigators for maintaining the AERONET sites at Kanpur and Beijing.

References

Brown, H., Liu, X., Pokhrel, R., Murphy, S., Lu, Z., Saleh, R., Mielonen, T., Kokkola, H., Bergman, T., Myhre, G., Skeie, R.B., Stier, P., Johnson, B., Bellouin, N., Schulz, M., Vakkari, V., Beukes, J.P., van Zyl, P.G., Liu, S., Chand, D., 2021. Biomass burning aerosols in most climate models are too absorbing. Nature Comm. 12, 277. https://doi.org/10.1038/s41467-020-20482-9.

Cherian, R., Quaas, J., 2020. Trends in AOD, clouds, and cloud radiative effects in satellite data and CMIP5 and CMIP6 model simulations over aerosol source regions. Geophys. Res. Lett. 47. https://doi.org/10.1029/2020GL087132 e2020GL087132.

Eck, T.F., Holben, B.N., Sinyuk, A., Pinker, R.T., Goloub, P., Chen, H., Chatenet, B., Li, Z., Singh, R.P., Tripathi, S.N., Reid, J.S., Giles, D.M., Dubovik, O., O'Neill, N.T., Smirnov, A., Wang, P., Xia, X., 2010. Climatological aspects of the optical properties of fine/coarse mode aerosol mixtures. J. Geophys. Res. 115, D19205. https://doi.org/10.1029/2010JD014002.

Eyring, V., Bony, S., Meehl, G.A., Senior, C.A., Stevens, B., Stouffer, R., Taylor, K.E., 2016. Overview of the coupled model intercomparison project phase 6 (CMIP6) experimental design and organization. Geosci. Model Dev. 9, 1937–1958.. https://doi.10.5194/gmd-9-1937-2016.

Gidden, M.J., Riahi, K., Smith, S.J., Fujimori, S., Luderer, G., Kriegler, E., van Vuuren, D.P., van den Berg, M., Feng, L., Klein, D., Calvin, K., Doelman, J.C., Frank, S., Fricko, O., Harmsen, M., Hasegawa, T., Havlik, P., Hilaire, J., Hoesly, R., Horing, J., Popp, A., Stehfest, E., Takahashi, T., 2019. Global emissions pathways under different socioeconomic scenarios for use in CMIP6: a dataset of harmonized emissions trajectories through the end of the century. Geosci. Model Dev. 12, 1443–1475. https://doi.org/10.5194/gmd-12-1443-2019.

Hoesly, R.M., Smith, J.S., Feng, L., Klimont, Z., Pitkanen, T., Siebert, J.J., Robert, L.V., Andres, R.J., Bolt, R.M., Bond, T.C., Dawidowski, L., Kholod, N., Kurokawa, J., Li, M., Liu, L., Lu, Z., Moura, M.C.P., O'Rourke, P., Zhang, Q., 2018. Historical (1750–2014) anthropogenic emissions of reactive gases and aerosols from the Community Emissions Data System (CEDS). . Geosci. Model Dev. 11, 369–408. https://doi.org/10.5194/gmd-11-369-2018.

Holben, B.N., Tanré, D., Smirnov, A., Eck, T.F., Slutsker, I., Abuhassan, N., Newcomb, W.W., Schafer, J.S., Chatenet, B., Lavenu, F., Kaufman, Y.J., Castle, J.V., Setzer, A., Markham, B., Clark, D., Frouin, R., Halthore, R., Karneli, A., O'Neill, N.T., Pietras, C., Pinker, R.T., Voss, K., Zibordi, G., 2001. An emerging ground-based aerosol climatology: Aerosol optical depth from AERONET. J. Geophys. Res. 106, 12067–12097.

IPCC, 2013. In: Stocker, T.F., Qin, D., Plattner, G.-K., Tignor, M., Allen, S.K., Boschung, J., Nauels, A., Xia, Y., Bex, V., Midgley, P.M. (Eds.), Summary for Policymakers in Climate Change 2013: The Physical Science Basis. Contribution of Working Group I to the Fifth Assessment Report of the Intergovernmental Panel on Climate Change. 2013. Cambridge Univ. Press, Cambridge, UK. And NY, USA, pp. 1–33.

IPCC, 2021. Summary for Policymakers. In: Climate Change 2021: The Physical Science Basis. In: Masson-Delmotte, V., Zhai, P., Pirani, A., Connors, S.L., Péan, C., Berger, S., Caud, N., Chen, Y., Goldfarb, L., Gomis, M.I., Huang, M., Leitzell, K., Lonnoy, E., Matthews, J.B.R., Maycock, T.K., Waterfield, T., Yelekçi, O., Yu, R., Zhou, B. (Eds.), Contribution of Working Group I to the Sixth Assessment Report of the Intergovernmental Panel on Climate Change. Cambridge University Press In Press.. IPCC 2021.

Jethva, H., Torres, O., Ahn, C., 2014. Global assessment of OMI aerosol single-scattering albedo using ground-based AERONET inversion. J. Geophys. Res. 119, 9020–9040.. https://doi:10.1002/2014JD021672.

Jethva, H., Torres, O., Field, R.D., Lyapustin, A., Gautam, R., Kayetha, V., 2019. Connecting crop productivity, residue fires, and air quality over northern India. Sci. Rep. 9. https://doi.org/10.1038/s41598-019-52799-x.

Kanaya, Y., Yamaji, K., Miyakawa, T., Taketani, F., Zhu, C., Choi, Y., Komazaki, Y., Ikeda, K., Kondo, Y., Klimont, Z., 2020. Rapid reduction in black carbon emissions from China: evidence from 2009–2019 observations on Fukue Island, Japan. Atmos. Chem. Phys. 20, 6339–6356. https://doi.org/10.5194/acp-20-6339-2020.

Katarzyna, B.T., Stolpe, M.B., Sippel, S., Fischer, E.M., Smith, C.J., Lehner, F., Knutti, R., 2020. Past warming trend constrains future warming in CMIP6 models. Sci. Adv. 6 (eaaz9549).

Kurokawa, J., Ohara, T., 2020. Long-term historical trends in air pollutant emissions in Asia: regional emission inventory in ASia (REAS) version 3. Atmos. Chem. Phys. 20, 12761–12793. https://doi.org/10.5194/acp-20-12761-2020.

Levy, R.C., Mattoo, S., Munchak, L.A., Remer, L.A., Sayer, A.M., Patadia, F., Hsu, N.C., 2013. The collection 6 MODIS aerosol products over land and ocean. Atmos. Meas. Tech. 6, 2989–3034.

Li, Z., Lau, W.K.-M., Ramanathan, V., Wu, G., Ding, Y., Manoj, M.G., Liu, J., Qian, Y., Li, J., Zhou, T., Fan, J., Rosenfeld, D., Ming, Y., Wang, Y., Huang, J., Wang, B., Xu, X., Lee, S.-S., Cribb, M., Zhang, F., Yang, X., Zhao, C., Takemura, T., Wang, K., Xia, X., Yin, Y., Zhang, H., Guo, J., Zhai, P.O.M., Sugimoto, N., Babu, S.S., Brassuer, G.P., 2016. Aerosol and monsoon climate interactions over Asia. Rev. Geophys. 54, 866–929 10.1002/2015R G000500.

Li, C., McLinden, C., Fioletov, V., Krotkov, N., Carn, S., Joiner, J., Streets, D., He, H., Ren, X., Li, Z., Dickerson, R.R., 2017. India is overtaking China as the world's largest emitter of anthropogenic sulfur dioxide. Sci. Rep. 7, 14304.

Myhre, G., Samset, B.H., Schulz, M., Balkanski, Y., Bauer, S., Berntsen, T.K., Bian, H., Bellouin, N., Chin, M., Diehl, T., Easter, R.C., Feichter, J., Ghan, S.J., Hauglustine, D., Iversen, T., Kinne, S., Kirkevåg, A., Lamarque, J.-F., Lin, G., Liu, X., Lund, M.T., Luo, G., Ma, X., van Noije, T., Penner, J.E., Rasch, P.J., Ruiz, A., Seland, Ø., Skeie, R.B., Stier, P., Takemura, T., Tsigardis, K., Wang, P., Wang, Z., Xu, L., Yu, H., Yu, F., Yoon, J.-H., Zhang, K., Zhang, H., Zhou, C., 2013. Radiative forcing of the direct effect from AeroCom phase II simulations. Atmos. Chem. Phys. 13, 1853–1877.

Myhre, G., Aas, W., Cherian, R., Collins, W., Faluvegi, G., Flanner, M., Forster, P., Hodneborg, Ø., Klimont, Z., Lund, M.T., Mülmenstädt, J., Myhre, C.L., Olivié, D., Prather, M., Quaas, J., Samset, B.H., Schnell, J.L., Schultz, M., Shindell, D., Skeie, R.B., Takemura, T., Tsyro, S., 2017. Multi-model simulations of aerosol and ozone radiative forcing due to anthropogenic emission changes during the period 1990–2015. Atmos. Chem. Phys. 17, 2709–2720.

O'Neill, B.C., Tebaldi, C., van Vuuren, D.P., Eyring, V., Friedlingstein, P., Hurtt, G., Knutti, R., Kriegler, E., Lamraque, J.-F., Lowe, J., Meehl, G.A., Moss, R., Riahl, K., Sanderson, B.M., 2016. The scenario model intercomparison project (ScenarioMIP) for CMIP6. Geosci. Model Dev. 9, 3461–3482.. https://doi.10.5194/gmd-9-3461-2016.

Ramachandran, S., Kedia, S., Sheel, V., 2015. Spatiotemporal characteristics of aerosols in India: observations and model simulations. Atmos. Environ. 116, 225–244.

Ramachandran, S., Rupakheti, M., Lawrence, M.G., 2020. Aerosol-induced atmospheric heating rate decreases over south and East Asia as a result of changing content and composition. Sci. Rep. 10, 20091. https://doi.org/10.1038/s41598-020-76936-z.

Ramanathan, V., Ramana, M.V., Roberts, G., Kim, D., Corrigan, C., Chung, C., Winker, D., 2007. Warming trends in Asia amplified by brown cloud absorption. Nature 448, 575–579.

Sadavarte, P., Venkataraman, C., 2014. Trends in multi-pollutant emissions from a technology-linked inventory for India: I Industry and transport sectors. 99, 353–364.

Samset, B.H., Lund, M.T., Bollasina, M., Myhre, G., Wilcox, L., 2019. 12, 582–586.

Torres, O., Bhartia, P.K., Jethva, H., Ahn, C., 2018. Impact of the ozone monitoring instrument row anomaly on the long-term record of aerosol products. Atmos. Meas. Tech. 11, 2701–2715. https://doi.org/10.5194/amt-11-2701-2018.

Wang, Z., Lin, L., Xu, Y., Che, H., Zhang, X., Dong, W., Wang, C., Gui, K., Xie, B., 2021. Incorrect Asian aerosols affecting the attribution and projection of regional climate change in CMIP6 models. npj Clim. Atmos. Sci. 4, 2. https://doi.org/10.1038/s41612-020-00159-2.

Zhang, X., Wang, Y.Q., Niu, T., Zhang, X.C., Gong, S.L., Zhang, Y.M., Sun, Y.J., 2012. Atmospheric aerosol compositions in China: spatial/temporal variability, chemical signature, regional haze distribution and comparisons with global aerosols. Atmos. Chem. Phys. 12, 779–799.

Zhao, A.D., Stevenson, D.S., Bollasina, M.A., 2019. The role of anthropogenic aerosols in future precipitation extremes over the Asian monsoon region. Clim. Dyn. 52, 6257–6278. https://doi.org/10.1007/s00382-018-4514-7.

Zheng, B., Tong, D., Li, M., Liu, F., Hong, C., Geng, C., Li, H., Li, X., Peng, L., Qi, J., Yan, L., Zhang, Y., Zhao, H., Zheng, Y., He, K., Zhang, Q., 2018. Trends in China's anthropogenic emissions since 2010 as the consequence of clean air actions. Atmos. Chem. Phys. 18, 14095–14111.